Solubility of CO_2 in water from -1.5 to $100\,°C$ and from 0.1 to 100 MPa: evaluation of literature data and thermodynamic modelling

Larryn W. Diamond[*], Nikolay N. Akinfiev

Institute of Geological Sciences, University of Bern, Baltzerstrasse 1-3, Bern CH-3012, Switzerland

Abstract

Experimental measurements of the solubility of CO_2 in pure water at pressures above 1 MPa have been assembled from 25 literature studies and tested for their accuracy against simple thermodynamic criteria. Of the 520 data compiled, 158 data were discarded. Possible reasons for the observed discrepancies between datasets are discussed. The 362 measurements that satisfy the acceptance criteria have been correlated by a thermodynamic model based on Henry's law and on recent high-accuracy equations of state. The assumption that the activity coefficients of aqueous CO_2 are equal to unity is found to be valid up to solubilities of approximately 2 mol%. At higher solubilities the activity coefficients show a systematic trend from values greater than unity at low temperatures, to values progressively lower than unity at high temperatures. An empirical correction function that describes this trend is applied to the basic model. The resulting corrected model reproduces the accepted experimental solubilities with a precision of better than 2% (1 standard deviation) over the entire P–T–x range considered, whereas the data themselves scatter with a standard deviation of approximately 1.7%. The model is available as a computer code at <www.geo.unibe.ch/diamond>. In addition to calculating solubility, the code calculates the full set of partial molar properties of the CO_2-bearing aqueous phase, including activity coefficients, partial molar volumes and chemical potentials.
© 2003 Elsevier Science B.V. All rights reserved.

Keywords: Carbon dioxide; H_2O; Model; Equation of state; Vapour–liquid equilibria; Activity coefficient

1. Introduction

Accurate description of the solubility of CO_2 in pure water is required in various scientific and technological fields, including the assessment of projects for CO_2 disposal on the sea floor or in sedimentary formations. Our particular interest lies in geochemical applications, especially in the analysis of CO_2-bearing fluid inclusions in minerals, e.g. [1,2]. For most of these applications, temperatures (T) up to $100\,°C$ and pressures (P) up to $100\,MPa$ are particularly relevant.

* Corresponding author.
E-mail address: diamond@geo.unibe.ch (L.W. Diamond).

A huge number of experimental studies have been conducted on CO_2 solubility in pure water. In 1991, Carroll et al. [3] and Crovetto [4] compiled and thermodynamically correlated the results for pressures below 1 MPa, and so only measurements from higher-pressure studies are considered here. To our knowledge, the last compilation and correlation of high pressure CO_2 solubilities at $T < 100\,°C$ was conducted in 1956 by Dodds et al. [5]. Many of the data are tabulated in the 1996 IUPAC Solubility Series volume [6], though without any discrimination of the conflicting measurements or attempt at correlation. Numerous experimental studies have been published since then, but important contradictions remain in the database. Although the publications generally state experimental uncertainties in CO_2 solubility to be on the order of only a few percent, comparison of different studies reveals disagreements of up to many tens of percent in solubilities measured under the same *P–T* conditions. Evidently there are unrecognised systematic errors in at least some of the studies, and therefore the data require evaluation and interpretation prior to their application. This paper presents such an analysis and a semi-empirical thermodynamic description of the data.

We first describe the relevant phase relations in the system and then apply criteria to discriminate the reliable from the unreliable experimental data. A basic thermodynamic model of CO_2 solubility in pure H_2O is then presented, founded on the traditional Henry's law approach of earlier workers. After evaluating the performance of the basic model we make an empirical correction to arrive at a precise description of the accepted data.

2. Phase equilibria

Fig. 1 illustrates the *P–T* region of concern in the present work, with respect to phase equilibria in the CO_2–H_2O system under conditions where water is stable. As will become apparent in the discussion further below, knowledge of the phase equilibria is important to interpret the significance of the experimental data and to define the limits of applicability of the present solubility model.

The equilibrium between CO_2-rich vapour (*V*) or liquid (L_{CO_2}) and the CO_2-bearing aqueous solution (L_{aq}) is limited at low temperatures and at elevated pressures by the stability field of solid CO_2-clathrate-hydrate, a non-stoichiometric compound with a nominal formula of $CO_2 \cdot 7.5H_2O$ [7–10]. Four-phase equilibria involving the clathrate are univariant in this system, and the corresponding quadruple points in *P–T* projection are labelled Q_1 and Q_2 (Fig. 1). At pressures and temperatures below Q_1 the coexistence of vapour and aqueous solution is limited by the stability field of ice.

The three-phase equilibrium between aqueous solution, CO_2-rich liquid and vapour (marked L_{aq}–L_{CO_2}– V in Fig. 1) runs very close to the liquid + vapour curve of pure CO_2, but at slightly lower pressures [10]. At temperatures below Q_2 the extension of the L_{aq}–L_{CO_2}–V curve is metastable (dashed in Fig. 1). For the purposes of this study, the *P–T* locus of the curve has been extrapolated to $0\,°C$ by extending the trend in pressure differences between the unary L_{CO_2}–V and binary L_{aq}–L_{CO_2}–V curves. At its high temperature end the L_{aq}–L_{CO_2}–V curve terminates at the lower critical end-point (LCEP) of the CO_2–H_2O binary. Song and Kobayashi [11] located the LCEP at 7.39 MPa and $31.05\,°C$, but here we plot the newer values of 7.411 MPa and $31.48\,°C$ measured by Wendland et al. [10]. The latter temperature is corroborated by the measurement of Morrison [12] at $31.424\,°C$. Thus, the LCEP is situated at slightly higher pressure and temperature than the critical point of pure CO_2 (7.3773 MPa, $30.9782\,°C$ [13]).

The upper critical curve of the CO_2–H_2O system, above which the two components are mutually soluble in any proportions, lies well outside the *P–T* region of this study at higher pressures and temperatures
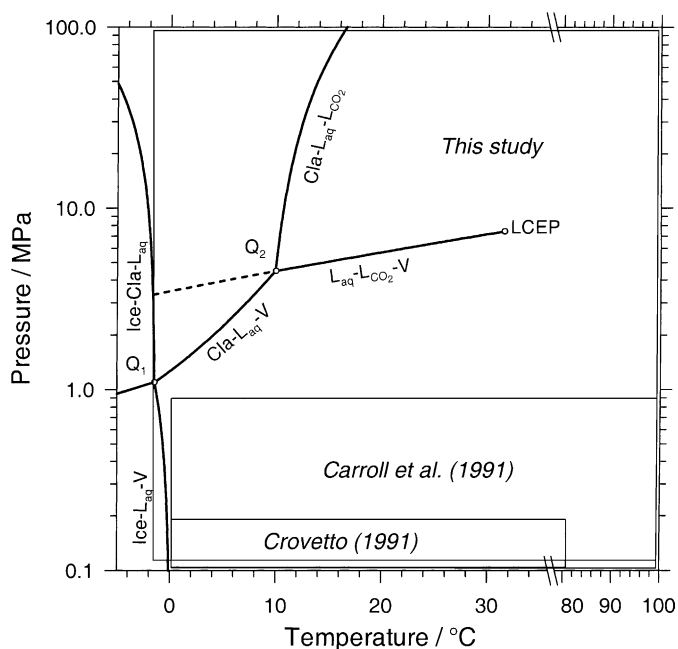
Fig. 1. Phase diagram of the CO_2–H_2O system in the pressure–temperature region relevant to this study, with water stable. LCEP denotes the lower critical end-point of the system. Quadruple point Q_1 involves equilibrium between H_2O-ice, CO_2-clathrate-hydrate, CO_2-bearing water and CO_2-vapour (Ice–Cla–L_{aq}–V). The quadruple point Q_2 marks equilibrium between CO_2-clathrate-hydrate, CO_2-bearing water, CO_2-liquid and CO_2-vapour (Cla–L_{aq}–L_{CO_2}–V). Phase boundaries for the pure H_2O end-member have been omitted for clarity. In the presence of excess H_2O the continuation of the L_{aq}–L_{CO_2}–V curve at temperatures below Q_2 is metastable (dashed). The *P–T* area covered by the present evaluation of aqueous CO_2 solubility (labelled *this study*) is shown relative to previous low-pressure compilations by Carroll et al. [3] and Crovetto [4]. Loci of phase boundaries are from [7–10].

[14–16]. This means that aqueous CO_2 solubilities are very low below 100 °C and 100 MPa, on the order of a few mol%.

3. Published experimental data

Twenty-five experimental studies within the region of interest are evaluated here (Table 1), comprising 520 data. Eleven of the publications are included in the 1996 IUPAC compilation [6]. The studies evaluated here span 120 years of investigation, the oldest work being by Wroblewski in 1883 [17] and the most recent by Anderson in 2002 [18]. In addition to these experimental data, we have also considered the 38 best-fit Henry's law constants reported by Carroll et al. [3] and Crovetto [4] for low pressures. These two fits are based on slightly different experimental databases but their results are very similar. Carroll et al. [3] processed data between 0 and 160 °C at pressures up to 1 MPa, whereas Crovetto fitted data between 0 and 80 °C at pressures up to 0.2 MPa. As the database of Carroll et al. overlaps most with our *P–T* region of interest, we have adopted their Henry constants to anchor our model at low pressure.

Table 1
Published studies of CO_2 solubility in pure water at 0–100 °C and 0.1–100 MPa

Reference	P_{total} (MPa)	T (°C)	Data	Method	P–T–x accuracy	w[a]
[17]	0.1–3.0	0–12.43	12	Vis., closed, $\Delta V(P, T)$	Not stated	0
[19][b]	2.4–16.7	20–60	34	Vis., closed, $\Delta V(P, T)$	$P \pm 0.05$ MPa, $T \pm 0.1$ °C, $x \pm 0.001$	0
[23]	0.1–5.3	0–15	18	Open, aq-extract, $V_{CO_2}(0.1, T_{lab})$	Not stated	0
[21]	0.5–3.0	20–30	10	Closed, aq-extract, $V_{CO_2}(0.1, T_{lab})$, aq-W	$P \pm 0.01$ MPa, T and x not stated	0
[32]	1.1–9.4	0–100	80	Closed, aq-extract, $V_{CO_2}(0.1, T_{lab})$	Irreproducibility at 100 °C and $P > 6$ MPa, T and x not stated	0.5
[35,36][c]	2.5–71	12–100	71	Closed, aq-extract, $V_{CO_2}(0.1, T_{lab})$	No P information, $T \pm 0.03$ °C, $x \pm 0.5\%$	1
[37]	0.1–2.0	10–30	15	Closed, aq-extract, $V_{CO_2}(0.1, T_{lab})$, aq-W	$P \pm 0.01$ MPa, No T or x information	1
[20]	2.5–7.6	20–35	20	Closed, aq-extract, GC	P calculated from T of bp of water, $T \pm 2.1$ °C	0
[38]	1.0–3.9	30–80	13	Open, aq-extract, gas-W	Averages of 2–4 Bunsen coefficients (α); $\alpha \pm 2\%$	1
[24]	1.0–4.6	0–25	12	Closed, aq-extract, gas-W	$P \pm 0.03\%$, $T \pm 0.06$ °C	0
[33]	4.96	25–75	11	Open, aq-extract, gas-W	$P \pm 0.3\%$, $T \pm 0.1$ °C, $x \pm 0.5\%$	0.5
[34]	4.96	25–100	7	Open, aq-extract, gas-W	$P \pm 0.3\%$, $T \pm 0.1$ °C, $x \pm 0.5\%$	0.5
[28][b]	10–80	50–100	9			0.33
[39]	0.5–4.6	50–100	9	Closed, $\Delta V(P, T)$	$P \pm 0.03\%$, $T \pm 0.005$ °C	1
[26]	0.8	33	1			0
[22]	0.7–20	16–93	16	Open, aq-extract, $V_{CO_2}(0.1, T_{lab})$	$P \pm 0.3\%$, $T \pm 0.1$ °C, $x \pm 1\%$	0.33
[29][d]	1.0–16	10–70	23			0.33
[40]	0.3–2.3	100	7	Closed, $\Delta V(P, T)$, EoS y by on-line GC	$P \pm 1$–2%, $T \pm 0.1$ °C, $x \pm 0.2$–1.1%	1
[3][e]	0.05–1.0	0–100	21 k_H			10
[4][e]	≤0.2	0–80	17 k_H			0
[41]	6.1–24.3	15–25	27	Open, separate phase recirculation; x_{CO_2} by "weighing"	P, T not stated, $x \pm 0.3\%$	1
[27]	6.4–29.5	5–20	24	Closed, vis., $\Delta V(P, T)$, EoS	$P \pm 0.01$ MPa, $T \pm 0.2$ °C, $x \pm 1.55\%$	0
[31][f]	2–8	25	9	Closed, vis., aq-extract, $V_{CO_2}(0.1, T_{lab})$	$P \pm 0.06$ MPa, $T \pm 0.05$ °C, $x \pm 7.7\%$	0.33
[42]	4–14	50–80	29	Open, vis., aq-extract, cold traps, $V_{CO_2}(0.1, T_{lab})$, aq-mass(0.1, T)	$P \pm 1.4\%$, $T \pm 0.1$ °C, $x \pm 1.4$–2.75%	1
[25]	2.0–4.2	3.9–10	9	Closed, vis., aq-extract via 25 nm filter; ρ_{aq}, $V_{CO_2}(0.1, T_{lab})$	$P \pm 0.08\%$, $T \pm 0.01$ °C $x \pm 3$–5%	0
[18]	0.1–2.2	1–15	54	Closed, $P(V_{total}, T)$, EoS	$P \pm < 0.6\%$, $T \pm 0.1$ °C, $x \pm 1\%$	1

Closed, open: closed or open system autoclave; vis.: phases visible in autoclave; $\Delta V(P, T)$: change in volume of phases measured at fixed P and T; aq-extract: aqueous phase extracted for degassing; $V_{CO_2}(0.1, T_{lab})$: volume of exsolved CO_2 measured at 0.1 MPa and laboratory temperature; aq-W, vap-W: aqueous or vapour phase analysed by wet-chemical method; GC: gas chromatography; EoS: solubility values depend on an equation of state; ρ_{aq}: density of degassed aqueous phase measured; $P(V_{total}, T)$: P measured at known total volume and T.

[a] Relative weight used in model fitting.

[b] Original publication not found, data from [6].

[c] Details of method in [50].

[d] Original publication not found, data from [30].

[e] Non-experimental.

[f] Solubilities provided by Kim Yangsoo (personal communication, 2002).

All the published solubility measurements were reduced to a common concentration basis of amount-of-substance fraction, i.e. "mole fraction". Scharlin [6] provides conversion factors for the variety of concentration and volumetric units used in the original literature. Experimental pressures are reported in some publications as partial pressures of CO_2 gas (P_{CO_2}). These values were recalculated here in terms of total pressures (P_{total}) by adding the pressure of saturated water vapour at the relevant temperature. Several publications do not state explicitly whether their pressures represent P_{CO_2} or P_{total}. In these cases we have deduced the meaning of "pressure" from the context of the described experimental methods. All the data are listed in their converted form in a text file available on the web-site <www.geo.unibe.ch/diamond>.

3.1. Criteria to discriminate experimental data

In the following we attempt to discriminate the reliable from the unreliable experimental data by assigning relative confidence factors, or weights (0, 0.33, 0.5 and 1.0, where 0 denotes rejection and 1.0 denotes high reliability). Four criteria of reliability were employed collectively for each published set of data; the first three are based on simple theoretical considerations, and the last one is based on practical expediency.

(1) In as much as the physicochemical properties of water and of carbon dioxide do not display discontinuities or oscillations in the *P–T* region of interest, any reliable set of experimentally determined CO_2 solubilities that spans a range of CO_2 pressures at fixed temperature should show a simple trend as a function of pressure.

(2) Regardless of the molecular interactions between CO_2 and H_2O in solution (the exact nature of which are poorly known), the unsymmetric activity coefficient of dissolved CO_2 ($\gamma_{CO_2(aq)}$) must approach unity as CO_2 solubility approaches zero. This criterion needs to be applied with caution in practice, because experimental uncertainties inherently increase as the solubility approaches zero. Nevertheless, at low finite solubilities, we expect reliable measurements to show only slight deviations of the activity coefficient of $CO_{2(aq)}$ from 1.0, and at higher solubilities any deviation should be gradual and systematic. We assumed the extent of deviation to be proportional to the difference between the experimental solubility values (expressed in terms of the Henry constant, see below) and the corresponding values given by Carroll et al. [3] and Crovetto [4].

(3) Confidence factors are reduced where stated experimental errors are large or where methodological problems are recognisable.

(4) After having applied the above criteria a good number of mutually conflicting studies still remained. We therefore used the simple principle of consensus (degree of mutual agreement) for discrimination, even though it provides no guarantee of accuracy. Thus, outliers from the general trends were rejected if the discrepancy was large, or assigned a low confidence factor if the discrepancy was relatively small. We note that the degree of consensus was the *only* criterion applied by Carroll et al. [3] and Crovetto [4] in evaluating the quality of the data they correlated.

To facilitate discussion of our assignment of confidence levels, Fig. 2 compares the 25 datasets (Table 2) as a function of CO_2 solubility, divided into convenient temperature intervals. Rejected data (factor zero) are shown in grey symbols and the accepted data are shown in black symbols. The accepted data are not differentiated graphically with respect to confidence levels. The ordinate in Fig. 2 represents the relative deviations of the experimental data from the thermodynamic models. As mentioned above, we initially took the CO_2 solubilities predicted by the low-pressure models of Carroll et al. [3] and Crovetto
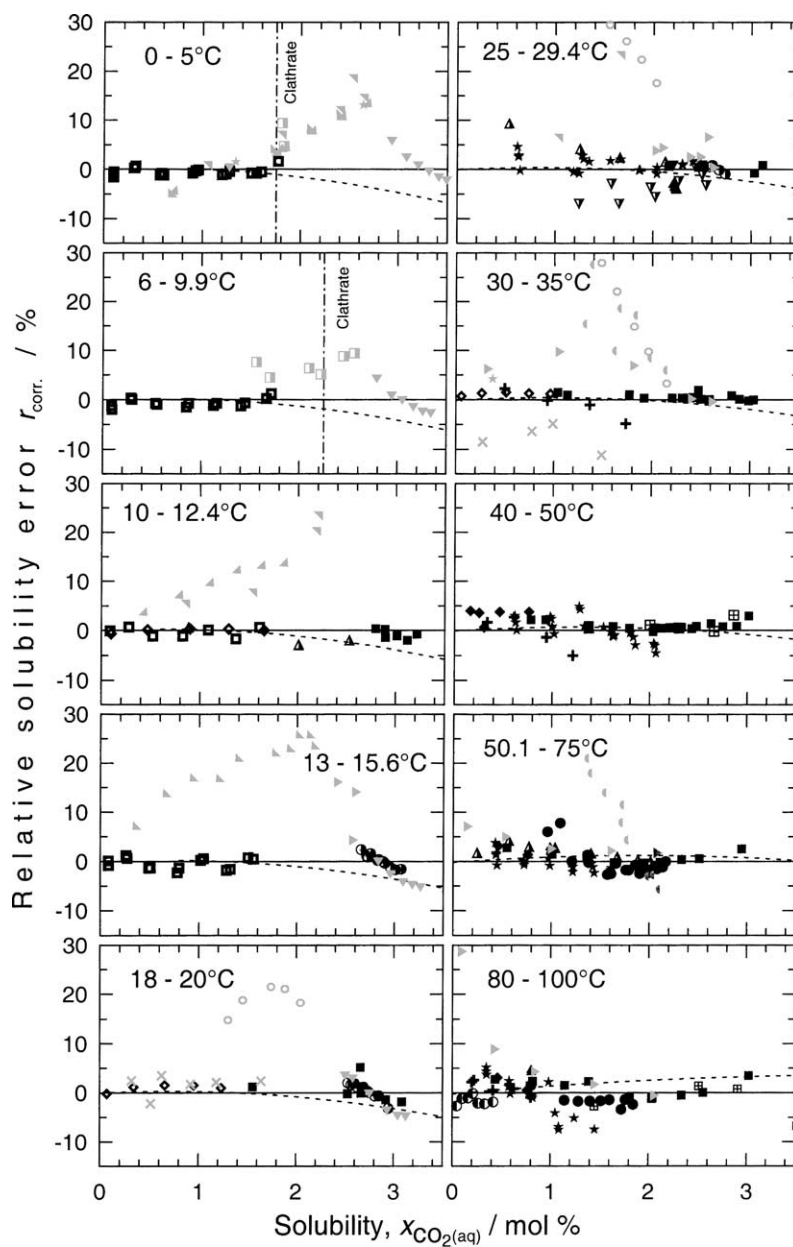
Fig. 2. Experimentally measured solubility of $CO_{2(aq)}$ (see symbols in Table 2) for selected temperature intervals, plotted against the relative deviation ($r_{corr.}$) of the model predictions. Solid curves: predictions of corrected model (Eq. (11)). Dashed curves: predictions of basic model (Eq. (6)) for median temperature of respective interval. Grey symbols denote experimental points rejected from model fitting (see text for explanation); black symbols denote accepted data.

Table 2
Symbols and model fitting weights of experimental data shown in Fig. 2

Symbol	Weight	Reference
◢	0	[17]
◖	0	[19]
◣	0	[23]
✕	0	[21]
★	0.5	[32]
■	1	[35,36]
◇	1	[37]
○	0	[20]
✚	1	[38]
◤	0	[24]
▲	0.5	[33]
▲	0.5	[34]
⊞	0.33	[28]
◆	1	[39]
✸	0	[26]
▶	0	[22]
△	0.33	[29]
◑	1	[40]
◐	1	[41]
▼	0	[27]
▽	0.33	[31]
●	1	[42]
◧	0	[25]
◨	1	[18]

[4] as the baseline for comparison. However, to avoid repeating Fig. 2 further on in this paper, we have plotted our final model results in Fig. 2 instead of the models of Carroll et al. and of Crovetto. Thus, the dashed curves, with intercepts at zero error, represent a fit to the weighted data with the constraint that $\gamma_{CO_2(aq)} = 1.0$ over the entire solubility range (curves are shown for the averages of the respective temperature intervals). The solid curves, which also show intercepts of zero error, represent a refined or "corrected" version of the basic model (described in detail below). The corrected model also observes the behaviour of $\gamma_{CO_2(aq)} \rightarrow 1.0$ as $x_{CO_2(aq)} \rightarrow 0$, and therefore the dashed and solid curves coincide at low solubilities.

At this stage of the evaluation of raw experimental data, the dashed and solid curves in Fig. 2 serve simply as convenient baselines for comparing the datasets against the discrimination criteria listed above (e.g. the data must approach zero error on the ordinate of Fig. 2 as $x_{CO_2(aq)} \rightarrow 0$). The precision of the models will be discussed in a following section.

3.2. Studies with factor zero

Examination of Fig. 2 shows that the data of Sander [19] and of Vilcu and Gainar [20] do not follow the expected trend of $\gamma_{CO_2(aq)} \rightarrow 1.0$ as concentration approaches zero. Furthermore, they display, by far, the greatest discrepancies with respect to the other studies (the deviations of 19 of the 33 data of

Sander lie off the scale of Fig. 2). The data of Kritschewsky et al. [21] and Gillespie and Wilson [22] are of relatively low precision and they deviate systematically from the majority of other studies. All four studies are therefore omitted from the fitting procedure.

Fig. 2 shows that, at temperatures below 10 °C, the earliest measurements of Wroblewski [17] are corroborated by the subsequent studies of Hähnel [23], Stewart and Munjal [24] and Servio and Englezos [25], though the latter studies are rather imprecise. Despite this corroboration, all the data imply very strong changes in the activity coefficient of $CO_{2(aq)}$ with increasing concentration. No other datasets contradict this trend at $T < 10$ °C, but nevertheless we suspect that all the data are affected by systematic errors related to the appearance of CO_2-clathrate-hydrate (Fig. 1; see Section 6 for details). We have therefore rated all four cited studies with a factor of zero.

Cramer [26] reports only one datum within our *P–T* region of concern, and this deviates perceptibly from the assumption of $\gamma_{CO_2(aq)} \rightarrow 1.0$ at low solubility. Without further data to characterise a set we have given this point zero weight.

The carefully conducted study by Teng et al. [27] claims to have measured the solubility of CO_2 in liquid-water in equilibrium with CO_2-clathrate-hydrate and CO_2-liquid, *over a range of pressures at fixed temperatures*. This apparently divariant phase assemblage violates the Gibbs phase rule (cf. Fig. 1), and so we have excluded the data for $T < 10$ °C from the final fitting (i.e. factor zero). The remainder of the Teng et al. [27] data overlap with the results of other studies at high pressure, but like the low-temperature data, they show an unusually sharp negative trend in Fig. 2, leading us to assign a confidence factor of zero for these data too.

3.3. Studies with factor 0.33

Fig. 2 displays data from [28] and [29], as cited in the IUPAC compilation [6] and in the handbook by Namiot [30], respectively. Our attempts to obtain the original publications failed and therefore, although the measurements appear fairly consistent with the other criteria, the lack of complete documentation caused us to treat the data with low confidence.

The solubilities reported by Yang et al. [31] for 25 °C deviate noticeably from those of most other studies, and the precision of the measurements is relatively low. Factor 0.33 thus seems appropriate for this study.

3.4. Studies with factor 0.5

Zel'vinskii (also spelled Zelvinskii, Zelvenskii or Zelvenski in the non-Russian literature) [32] provides the largest number of measurements of all the studies evaluated here, and the experiments cover the entire temperature range of interest. For the runs at 0 °C, Zel'vinskii deduced that clathrate must have been present at pressures above 1 MPa. These, and the lower-pressure data at 0 °C, deviate strongly from the assumption of $\gamma_{CO_2(aq)} = 1.0$ and therefore we omitted all the 0 °C values from our fitting. Above 50 °C the measurements of Zel'vinskii do not converge on $\gamma_{CO_2(aq)} = 1.0$ at low CO_2 concentrations, and in general the internal reproducibility of the data is poorer than more recent studies. Nevertheless, the solubility values at intermediate temperatures (25–40 °C) agree with the majority of other studies remarkably well; and hence, we assigned all the values above 0 °C a factor of 0.5.

Solubility measurements by Malinin and Savelyeva [33] and Malinin and Kurovskaya [34] show fairly good reproducibility but they deviate from most other data. Malinin and co-workers admit that their

solubilities in pure H_2O may not be very accurate, because their experimental apparatus was designed principally to measure the *difference* in CO_2 solubility between pure H_2O and aqueous salt solutions. We therefore assigned a factor of 0.5 to these two studies.

3.5. Studies with factor 1.0

Nine studies remain (i.e. [18,35–42]), which appear to satisfy all the discrimination criteria, and which agree fairly well with each other. In detail there are indeed discrepancies between these datasets, but we found no justification or means to differentiate them further. All were therefore assigned the highest confidence factor of 1.0.

3.6. P–T coverage of accepted experimental data

The distribution of the accepted experimental data in *P–T* space is shown in Fig. 3. It can be seen that coverage is dense at low pressures and over the entire temperature range of interest, but coverage is extremely sparse above 50 MPa. Only one datum [35] has been retained within the clathrate stability field (to the left of the clathrate dissociation curve labelled $Cla–L_{aq}–L_{CO_2}$ in Fig. 3a; see Section 6 for details).

4. Basic model of aqueous CO_2 solubility

Having eliminated much of the scatter in the experimental database by rejecting several studies, we now present a thermodynamic model to describe the 362 accepted data. The solubility of CO_2 in water is modelled according to the following reaction equilibrium:

$$CO_{2(vap,\,liq)} = CO_{2(aq)}, \tag{1}$$

where $CO_{2(vap,liq)}$ stands for carbon dioxide in the CO_2-rich vapour or liquid phase, and $CO_{2(aq)}$ denotes all aqueous species of CO_2 lumped together. The influence of products of CO_2 hydrolysis (HCO_3^-, CO_3^{2-}) on aqueous CO_2 solubility is negligible in the *P–T* region of interest [43].

As traditionally approached by many other workers (e.g. [3,4,40,41]), the solubility implied by reaction (1) can be expressed in terms of the Henry's law constant as follows:

$$x_{CO_2(aq)} = \frac{f^0_{CO_2(P,T)} y \gamma_y}{k_{H(P,T)} \gamma_{CO_2(aq)}}, \tag{2}$$

where $x_{CO_2(aq)}$ and y are the mole fractions of CO_2 in the aqueous and non-aqueous phases, respectively, $k_{H(P,T)}$ (in MPa) is the Henry constant of CO_2 in pure water on a mole fraction basis at specified *P–T* conditions, $f^0_{CO_2(P,T)}$ is the fugacity (in MPa) of pure CO_2 at specified *P–T* conditions, $\gamma_{CO_2(aq)}$ is the unsymmetric (Henry's law) activity coefficient of aqueous CO_2, such that $\gamma_{CO_2(aq)} \to 1$ as $x_{CO_2(aq)} \to 0$, and γ_y is the symmetric (Raoult's law) activity coefficient of CO_2 in the non-aqueous phase, such that $\gamma_y \to 1$ as $y \to 1$. Note that, as k_H includes the pressure-dependence, no Poynting correction is required.

Solubilities are calculated from Eq. (2) using the following methods and assumptions:

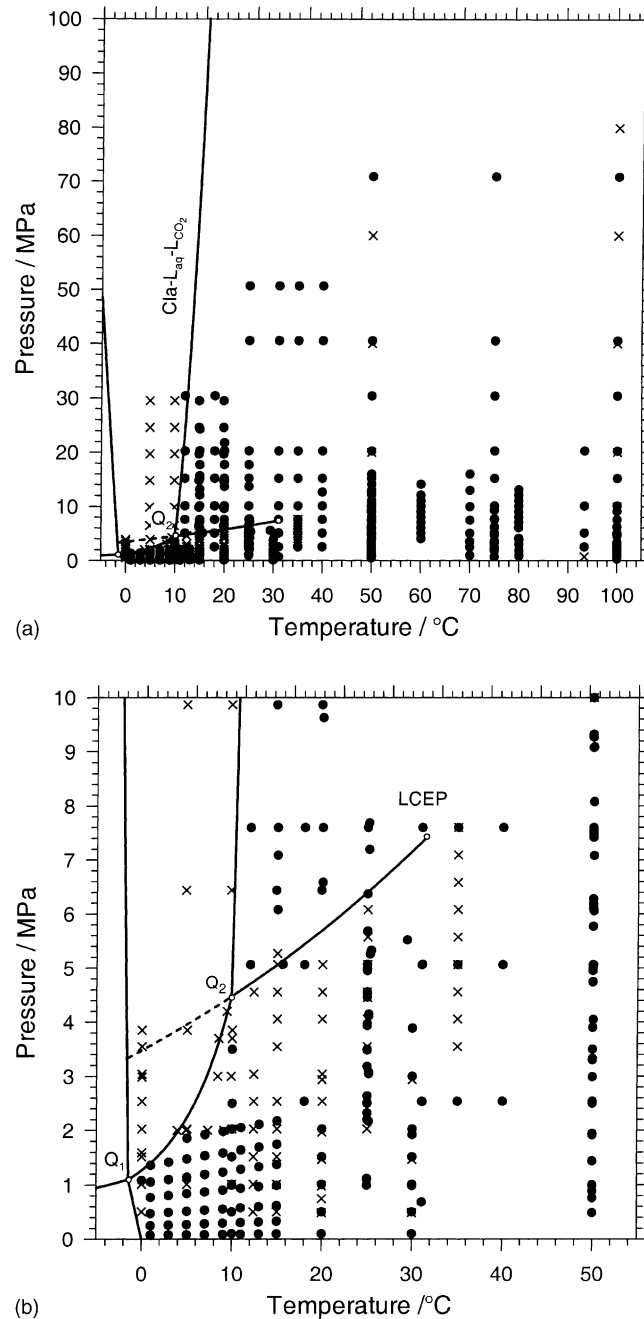1. $\gamma_{CO_2(aq)}$ and γ_y are assumed equal to unity.

Fig. 3. *P–T* distribution of the 520 experimental data on aqueous CO_2 solubility considered in this study. Phase boundaries are as defined in Fig. 1. Dots show the 362 accepted data (weight > 0), crosses show the 158 rejected data (weight = 0). Data sources are differentiated in Fig. 2. (a) Entire *P–T* region of model fit; (b) detail of low-*P*, low-*T* region. Note that coverage of the fit region is extremely sparse at $P > 50$ MPa and that only one point is retained within the stability field of CO_2-clathrate (left of the curve labelled Cla–L_{aq}–L_{CO_2} in (a); see text for details).

2. $f^0_{CO_2(P,T)}$ for the CO_2-rich vapour and for the CO_2-rich liquid are calculated from the equation of state of Span and Wagner [13], which is accurate to within 0.05% over the *P–T* range of interest, including the near-critical region of CO_2.

3. *y* is estimated from two approximations; at low pressures the vapour is assumed to be an ideal solution of non-ideal gases, according to the Lewis–Randall rule:

$$y = 1 - \frac{P_{\text{watersat}}}{P_{\text{total}}}, \tag{3}$$

where P_{watersat} is the pressure of liquid–vapour equilibrium of pure H_2O (in MPa) and P_{total} is the total pressure (in MPa), all at specified temperature. At high pressures, *y* is estimated roughly from experimental data [41,44] fitted to the following empirical equation:

$$y = 1 - (0.1256t - 0.0212) \times 10^{-3} - P(0.065t + 1.121) \times 10^{-5} \tag{4}$$

where *t* is temperature in °C and *P* is pressure in MPa.

   The switch-over between use of Eqs. (3) and (4) is taken to be their points of intersection. The relative error in CO_2 solubility calculated from Eqs. (3) and (4) due to the uncertainty in *y* is estimated to be less than 0.2%. Owing to their approximate nature, Eqs. (3) and (4) are not recommended for use outside the context and *P–T* limits of the present study.

4. k_H is calculated from the virial-like equation of state of Akinfiev and Diamond [45]:

$$\ln(k_H) = (1 - \xi) \ln f^0_{H_2O} + \xi \ln \left(\frac{RT}{M_w} \rho^0_{H_2O} \right) + 2\rho^0_{H_2O} \left[a + b \left(\frac{1000}{T} \right)^{0.5} \right], \tag{5}$$

where $f^0_{H_2O}$ is the fugacity (in MPa) and $\rho^0_{H_2O}$ is the density (in g cm^{-3}) of pure water calculated using the equation of state of Hill [46] at specified *P* and *T*, *R* (8.31441 cm^3 MPa K^{-1} mol^{-1}) is the gas constant, *T* is temperature (in K), M_w is the molar mass of H_2O (18.0153 g mol^{-1}), and ξ (dimensionless), *a* (in cm^3 g^{-1}) and *b* (in cm^3 K$^{0.5}$ g^{-1}) are empirical fit parameters. In the present case, ξ, which is a scaling factor for the volume of the dissolved molecules, is held constant at -0.088 to keep the standard partial molar volume of aqueous CO_2 close to the experimentally observed value (32.8 cm^3 mol^{-1} at 25 °C, 0.1 MPa, [47]). Values of the *a* and *b* parameters for CO_2–H_2O mixtures were derived by Akinfiev and Diamond [45] from experimentally determined Henry constants spanning a very wide temperature range. Here, to improve accuracy for the narrower range between 0 and 100 °C, the *a* and *b* parameters were fitted statistically to our experimental database as follows:

   4.1. The 21 values of Henry constants listed in 5° intervals by Carroll et al. [3] for the range 0–100 °C at 0.1 MPa were used to anchor our fit at the low-pressure limit of our study. Each of the 21 values was assigned a statistical weight of 10.

   4.2. Henry constants were calculated from Eq. (2) for all the experimental data on CO_2 solubility that we have evaluated above, assuming $\gamma_{CO_2(aq)} = 1$ and $\gamma_y = 1$. Each datum was assigned a statistical weight equal to its confidence factor (0, 0.33, 0.5 or 1.0; Table 1).

   4.3. The *a* and *b* parameters of the equation of state were then fitted only to the set of Henry constants pertaining to measured solubilities *less than* 2 mol% $CO_2(aq)$. This restriction was adopted to avoid inducing errors in *a* and *b* from high-solubility data, which seem to require deviations of $\gamma_{CO_2(aq)}$ from our assumed value of 1 (see discussion below). In other words, all the experimental data for solubilities above 2 mol% $CO_2(aq)$ were ignored at this stage, regardless of their confidence factors.

4.4. Fitting was performed by the conventional weighted least-squares method, resulting in:

$$a = -9.3134 \, cm^3 \, g^{-1}, \qquad b = 11.5477 \, cm^3 \, K^{0.5} \, g^{-1}.$$

For comparison, the earlier values given by Akinfiev and Diamond [45] for a wider temperature range are $a = -8.8321$ and $b = 11.2684$. Using the new values, Eq. (2) yields k_H values for 0.1 MPa that deviate from those of Carroll et al. [3] by only 0.76% (1 standard deviation). Carroll et al. [3] did not estimate the standard deviation of the raw experimental data they evaluated, but Crovetto [4] quotes values above 1.1% for a similar database at 0.1 MPa. The above fitting of the a and b parameters thus reproduces the values in the Carroll et al. study within the level of experimental certainty.

4.1. Precision of the basic model

The relative error in CO_2 solubility associated with our basic model (Eq. (2)) is defined as:

$$r_0 \equiv \frac{x_{model} - x_{exper.}}{x_{exper.}}, \tag{6}$$

where x_{model} and $x_{exper.}$ are the predicted (Eq. (2)) and experimental CO_2 solubilities for a specific datum, respectively. The weighted standard deviation of the relative solubility errors, σ, is calculated from:

$$\sigma = \left(\frac{\sum_i w_i r_0^2}{\sum_i w_i - 1} \right)^{0.5}, \tag{7}$$

where w_i is the weight assigned to datum i. Solution of Eq. (7) shows that the basic model fits all the accepted experimental data (i.e. those with non-zero confidence factors) with a standard deviation of 2.4% (Fig. 4).

The standard deviation of the basic model increases noticeably when only the experimental data for high CO_2 solubilities are entered into Eq. (7). Fig. 4 shows that $\sigma = 3.1\%$ when only the data with $x_{CO_2(aq)} > 0.025$ are considered, and $\sigma = 2.7\%$ when only data with $x_{CO_2(aq)} > 0.020$ are considered. Inclusion of more data at lower solubilities changes σ insignificantly. This suggests that the basic model is a good fit in the low-solubility region ($x_{CO_2(aq)} < 0.020$), but that it is only moderately good at high solubilities. The same behaviour is visible in Fig. 2, where the dashed curves show the deviation of the basic model from the depicted data. The basic model tends to overestimate the experimental solubilities in the high-pressure, low-temperature region, and it tends to underestimate the experimental values in the high-pressure, high-temperature region.

5. Corrected model of aqueous CO_2 solubility

In order to improve the performance of the model at higher solubilities, an empirical correction has been made to the values calculated from Eq. (2). The solubility errors relative to the basic model were fitted by weighted non-linear regression as a function of CO_2 concentration and temperature. Care was taken to anchor the origin of the fit to zero error at zero $CO_{2(aq)}$ solubility. In order to find the best mathematical
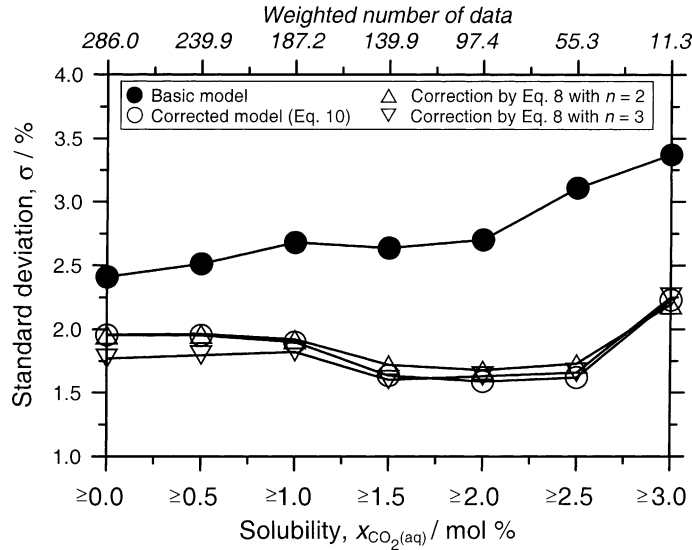
Fig. 4. Precision of various model fits to the accepted experimental data on CO_2 solubility. Precision is expressed as the standard deviation (σ) of the weighted relative errors (Eq. (7)). The lower x-axis shows the cumulative subsets of experimental data used to calculate σ. The upper x-axis shows the weighted number of data in the respective subsets. Thus, points at "≥3.0" display the precision with which the models fit the 11.3 weighted data with $3.0 \leq x_{CO_2(aq)} \leq 3.52$ mol%; points at "≥2.5" data display the precision with which the model fits the 55.3 weighted data with $2.5 \leq x_{CO_2(aq)} \leq 3.52$, and so on. Points at "≥0.0" denote the entire dataset, i.e. $0.0 \leq x_{CO_2(aq)} \leq 3.52$ (286 weighted data). The fit of the basic model (●) is appreciably improved by applying corrections of the type given in Eq. (8), especially at high solubilities (open symbols). The preferred correction (Eq. (10); ○) reduces σ for the entire dataset to just under 2%. See text for further explanation.

description, the form of the three-dimensional surface, representing the relative errors, was varied from simple to complex polynomial expressions of the type:

$$r^* = \sum_{i=0}^{n}\sum_{j=0}^{n} a_{ij} t^i x_{model}^j, \tag{8}$$

where a_{ij} denotes the polynomial coefficients, t is temperature in °C, x_{model} is the CO_2 solubility in mol% calculated by the basic model, and $n = 2$ or 3.

The relative errors, or residuals (in mol% CO_2), calculated from the best-fit expressions, such as (8), were then added to the solubilities calculated by the basic model (Eq. (2)). The resulting "corrected" predictions are compared in terms of σ values in Fig. 4. All of the corrections yield significant improvements to the basic model. Thus, the standard deviation for data with $x_{CO_2(aq)} > 0.025$ drops from 3.1 to around 1.6–1.7%, depending on the complexity of the chosen polynomial. When all the accepted experimental data are considered ($x_{CO_2(aq)} > 0$), the overall standard deviation drops from 2.4 to 1.77–1.95%. The higher-order polynomials bring the best performance (1.77%), and indeed values around 1.7% represent the limit of scatter in the original experimental data. Unfortunately, the higher-order polynomials do not behave suitably when extrapolated outside the fit region (e.g. at $T > 100$ °C) and therefore we have chosen to employ one of the simplest of the polynomial descriptions tested (open circles in Fig. 4), which

is linear in temperature and which yields an overall deviation of just under 2%:

$$r^* = 3.63579 \times 10^{-5} - 4.477820 \times 10^{-6}t + 1.18833 \times 10^{-4}tx_{\text{model}} + 5.41469 \times 10^{-5}tx_{\text{model}}^2$$
$$+ 7.31010 \times 10^{-3}x_{\text{model}} - 7.49356 \times 10^{-3}x_{\text{model}}^2, \tag{9}$$

where r^* is the best fit to the residual error of the basic model, t is temperature in $^\circ$C between 0 and 100 $^\circ$C, and x_{model} is the CO_2 solubility in mol% ($0 < x_{\text{model}} < 4$) calculated by the basic model at specified temperature (Eq. (2)). Thus, the corrected CO_2 solubility $x_{\text{corr.}}$ is given by the following equation:

$$x_{\text{corr.}} = x_{\text{model}}(1 + r^*). \tag{10}$$

The corrected CO_2 solubilities are denoted by the solid "zero error" reference lines in Fig. 2. The relative error depicted in Fig. 2, $r_{\text{corr.}}$, is now defined as:

$$r_{\text{corr.}} \equiv \frac{x_{\text{corr.}} - x_{\text{exper.}}}{x_{\text{exper.}}} = r_0(1 + r^*). \tag{11}$$

We note that the correction function, r^*, can be used to derive the Henry's law activity coefficient of aqueous CO_2 on a mole-fraction scale, γ_H. Thus, rearranging Eq. (10):

$$\gamma_H = \frac{x_{\text{model}}}{x_{\text{corr.}}} = (1 + r^*)^{-1}. \tag{12}$$

This activity coefficient can in turn be converted to the Henry's law molal concentration scale, as detailed in Appendix A (Eq. (A.5)), yielding a convenient expression for the temperature- and concentration-dependence of the molal-scale activity coefficient (Eq. (A.6)).

To facilitate application of the corrected model, polynomial functions are provided in Appendix B (Eqs. (B.1)–(B.4)) to describe CO_2 solubilities along the stability curves of clathrate and ice and along the L_{aq}–L_{CO_2}–V element (cf. Fig. 7).

6. Discussion

6.1. Accuracy of experimental data

Henry's law has a long history of success in application to dissolved gas species at very low concentrations. There is therefore little doubt that the datasets which scatter wildly in Fig. 2, or for which the activity coefficients, $\gamma_{CO_2(aq)}$, do not approach unity at low solubilities, should indeed have been rejected from our fitting procedure. Even at higher solubilities ($x_{CO_2(aq)} > 0.01$), as long as the experimental data obey the assumption that $\gamma_{CO_2(aq)} = 1.0$, there seems to be no need to question their accuracy. We are therefore confident that our rejection of the conflicting datasets at $x_{CO_2(aq)} > 0.01$ and at $T > 10\,^\circ$C (Fig. 2) is valid. More open to discussion is our rejection of measurements for $x_{CO_2(aq)} > 0.0175$ at temperatures below 10 $^\circ$C. Here we have rejected *all* the available studies (i.e. [17,19,20,23–25]), because they do not follow the extrapolation of the trend in $\gamma_{CO_2(aq)}$ observed at *higher* temperatures. The discarded studies are disconcertingly reproducible and they span 120 years of developments in experimental methods, i.e. they show qualities which conventionally would suffice to confirm experimental accuracy. However, we argue that all the published data for $x_{CO_2(aq)} > 0.0175$ at $T < 10\,^\circ$C are affected by serious systematic errors, which are more or less reproducible.

In searching for explanations for these gross disagreements, we reviewed the methods of the 25 evaluated studies (summarized chronologically in Table 1). The most discrepant study of all is that by Vilcu and Gainar [20]. Presumably their errors arise from their estimates of pressure, which are not based on direct measurements but are calculated from the effect of their experimentally induced pressure on the boiling point of pure water. Zel'vinskii [32] also apparently had problems with pressure determinations (see discussion in [36]). Apart from these cases it does not seem possible to assess retrospectively the possible errors in pressure, temperature or CO_2 analysis in the various publications. The broad agreement between the data for $x_{CO_2} > 0.0175$ at $T < 10\,^{\circ}C$ in fact suggests that these measurable quantities were not the source of the systematic errors.

It is notable that most of the aberrant measurements at $T < 10\,^{\circ}C$ were made within or close to the stability region of CO_2-clathrate-hydrate (Fig. 1; see also boundaries marked on low-temperature plots in Fig. 2). Whereas some experimental apparatuses were specifically designed to view the clathrate directly (e.g. [25]), other set-ups precluded its detection (e.g. [23]) or only allowed for indirect and uncertain deduction of its presence (e.g. [32]) (Table 3). In the latter cases there is a possibility that solid clathrate was inadvertently entrained in the aqueous solution separated for analysis. However, this alone cannot explain the low CO_2 values of the rejected studies, because the clathrate molecule, with a nominal formula of $CO_2 \cdot 5.75H_2O$, has a higher CO_2:H_2O ratio than the coexisting aqueous solution. Several studies have in fact shown that the solubility of CO_2 in water in divariant equilibrium with clathrate is much lower than in water in the absence of clathrate [25,31,48,49]. Unwitting analysis of this depleted aqueous solution could perhaps explain the anomalously low solubilities of the rejected studies. On the other hand, low solubilities are also reported in some of the rejected studies at P–T conditions outside the clathrate stability field ($T > 10\,^{\circ}C$ in Fig. 2). Thus, although problems related to the presence of clathrate in the experiments probably contribute to the discrepancies, other factors must be involved too.

A second experimental issue arising from the examination of experimental methods is that of reaction kinetics. Relevant information was found in only 13 of the reviewed studies (Table 3). Comparison of the reaction times allowed prior to water sampling shows no obvious pattern; the rejected studies report equilibration times between 6 h [23] and 24 h [25,27], while the accepted studies allowed between 30 min (dynamic recirculation method of King et al. [41]) to 48 h [33,35,36]) for equilibration. Nearly all the studies report using some form of agitation of the reactants in the experimental vessels. Most of the experiments were designed to approach equilibrium by allowing CO_2 to diffuse into water which was under-saturated with respect to CO_2 (Table 3). Among these studies are all those that were rejected according to the above criteria, but three studies that were assigned a confidence factor of 1.0 are also included. Two studies [18,37], both rated with a confidence factor of 1.0, approached equilibrium via exsolution of CO_2 from the over-saturated state. Finally, only three groups reported to have reversed all their experiments (i.e. approached equilibrium from over-saturated and under-saturated states): Wroblewski [17], whose study was rejected (this study probably suffered from influence of clathrate as well), Malinin and co-workers [33,34], whose studies were not designed specifically to measure accurate solubilities in the CO_2–H_2O binary system, and Wiebe and Gaddy [35,36], as described in [50]. Malinin and Savelyeva [33] emphasize that initially under-saturated water becomes saturated in CO_2 only very slowly, especially at low temperatures and with large volumes of water, and this view is underscored by the huge experimental effort expended by Wiebe and Gaddy [35,36] and by King et al. [41] to achieve equilibrium at low temperatures and high pressures. A definitive judgement on the role of kinetics is not possible at this stage, as so many of the evaluated publications contain no mention of these issues. Nevertheless, kinetics appear to be of fundamental importance for solubility measurements at low temperatures and

Table 3
Experimental details relevant to CO_2–H_2O equilibration

Reference	Approach to equilibrium	Agitation	Equilibration time	CO_2-hydrate-clathrate
[17]	Reversed from high and low P_{CO_2}	Shaking	Not stated	Observed at $0\,°C$ at $P > 3\,MPa$
[19][a]				
[23]	From high P_{CO_2}; CO_2 dissolution into under-saturated water	Shaking	6 h	Undetectable by apparatus
[21]	From high P_{CO_2}; CO_2 dissolution into under-saturated water	Bubbling CO_2 gas	"Hours"	Inapplicable P–T conditions
[32]	Isothermal increase of P_{CO_2}; CO_2 dissolution into under-saturated water	Bubbling CO_2 gas	Not stated	Undetectable by apparatus; presence at $0\,°C$, $P > 1\,MPa$ deduced indirectly; all data for $0\,°C$ (rejected in this study) apparently in presence of clathrate
[35,36]	Reversed from high and low P_{CO_2}	Bubbling CO_2 gas	"Several hours to days"	Undetectable by apparatus; presence at $10\,°C$, $P > 5\,MPa$ and $12\,°C$, $P > 30\,MPa$ deduced indirectly; presence at other P–T conditions not excluded
[37]	From low P_{CO_2}; CO_2 exsolution from over-saturated water	Shaking and stirring	Not stated	Inapplicable P–T conditions
[20]	Not stated	Stirring	Not stated	Inapplicable P–T conditions
[38]	Constant P_{CO_2} maintained by pumping against dissolution of CO_2 into under-saturated water	Rocking	Open for 1 h; closed for 1 h	Inapplicable P–T conditions
[24]	From low P_{CO_2}; CO_2 dissolution into under-saturated water; checked from high P_{CO_2} in a few runs	Rocking	4 h	Undetectable by apparatus; clathrate stability field at $P \geq 5\,MPa$ deliberately avoided
[33]	Reversed from high and low P_{CO_2}	Bubbling CO_2 gas	48 h at 25 and $50\,°C$; 24 h at $75\,°C$	Inapplicable P–T conditions
[34]	Reversed from high and low P_{CO_2}	Bubbling CO_2 gas	48 h at 25 and $50\,°C$; 24 h at $75\,°C$	Inapplicable P–T conditions
[28][a]		Rocking		
[39]	Not stated	Not stated	Not stated	
[22]	Not stated	Rocking	Not stated	Inapplicable P–T conditions
[29][b]				Inapplicable P–T conditions
[40]	Fixed V and T; P_{total} measured after CO_2 dissolution into under-saturated water	Stirring	12 h	Inapplicable P–T conditions
[41]	Constant P_{CO_2} maintained by pumping against dissolution of CO_2 into under-saturated water	Stirring then bubbling CO_2 gas	20–30 min for final recirculation	Inapplicable P–T conditions
[27]	Diffusion of liquid CO_2 through clathrate layer into under-saturated water	Deliberate fluctuation of P_{CO_2}	24 h	Observed optically at $T = 10\,°C$

Table 3 (*Continued*)

Reference	Approach to equilibrium	Agitation	Equilibration time	CO_2-hydrate-clathrate
[31]	Mechanical mixing: dissolution of CO_2 into under-saturated water	Stirring and water circulation	8 h	Observed optically
[42]	Mechanical mixing: dissolution of CO_2 into under-saturated water	Throttling of phases through tortuous path	Not stated	Inapplicable *P–T* conditions
[25]	From low P_{CO_2}; CO_2 dissolution into under-saturated water	Stirring	24 h	Observed optically; filtered from sampled aqueous phase prior to analysis
[18]	Initial isochoric cooling (CO_2 dissolution into under-saturated water); then isochoric heating (CO_2 exsolution from over-saturated water)	Gas-entraining stirrer	1–2 h	Undetectable by apparatus; clathrate stability field deliberately avoided

[a] Original publication not found; information from [6].

[b] Original publication not found; information from [30].

high pressures. Further time-resolved experiments in the *P–T* region close to clathrate stability seem necessary to resolve these questions.

Finally, we note that our evaluation of accuracy of the studies at elevated pressures leads to conclusions that are similar to those of Carroll et al. [3] and Crovetto [4] for low-pressure experiments. For $P < 1$ MPa, Carroll et al. [3] also found that the studies of Hähnel [23] and Gillespie and Wilson [22] agreed poorly, and that those of Wroblewski [17], Zel'vinskii [32] and Stewart and Munjal [24] agreed only moderately well, with the great majority of the 80 studies they reviewed. Similarly, the data of Bartholomé and Friz [37], Matous et al. [38], Müller et al. [40] and Zawisza and Malesinska [39] all showed excellent agreement with the majority of compiled data.

6.2. Accuracy of the CO₂ solubility models

As stated above, our basic model (Eq. (2)) assumes that the activity coefficient of $CO_{2(aq)}$, $\gamma_{CO_2(aq)}$, is equal to unity over the entire solubility range under discussion. This assumption works well at all temperatures up to CO_2 solubilities of approximately 2 mol% (the predictions of the basic and corrected models are indistinguishable at $x < 0.02$, Fig. 2). Our corrected model empirically accounts for the deviation of the accepted solubility data from this assumption. At $x_{CO_2} > 0.02$ the corrected model (continuous lines in Fig. 2) implies, via Eq. (2), that $\gamma_{CO_2(aq)}$ is greater than 1.0 at temperatures below about 50 °C, with the deviations increasing steadily with decreasing temperature. At temperatures progressively higher than 50 °C, the implied values of $\gamma_{CO_2(aq)}$ become progressively smaller than 1.0. The experimental data thus define a consistent, monotonic trend in $\gamma_{CO_2(aq)}$ throughout the temperature interval considered, as described by Eq. (9). We offer no explanation as to why $\gamma_{CO_2(aq)}$ should increase progressively above 1.0 at low temperatures and high pressures, and we emphasize that the corrected model is only an extrapolation for $x_{CO_2} > 0.0175$ at $T < 10$ °C, and is therefore to be treated with caution. Moreover, the fit of the corrected model at $T < 50$ °C and at elevated pressures is determined largely by the studies of Wiebe

and Gaddy [35,36] and of King et al. [41]. One could therefore question whether this implied trend in $\gamma_{CO_2(aq)}$ represents a real property of the aqueous solutions, or whether the corrected model simply over-fits experimental data that have a relatively high uncertainty. On the other hand, the deviations do not come as a surprise, as any model based on Henry's law is doomed to fail at some point as solubilities increase. Assuming that the accepted high-pressure experimental data are accurate, the point at which the Henryan model fails in the present case is approximately 2 mol% $CO_2(aq)$.

Figs. 5–7 and Eq. (B.1) (Appendix B) define the model CO_2 solubility along the L_{aq}–L_{CO_2}–V co-existence curve. Although the accepted experimental data constrain the solubilities along this curve, it should be noted that none of the 362 accepted data were actually measured in the presence of this three-phase assemblage. In fact, the experimental data alone do not even define the sharp kinks in the solubility curves shown along the L_{aq}–L_{CO_2}–V curve in Figs. 5–7. However, there is good reason to accept that such kinks do indeed exist, dictated via Eq. (1) by the kinks in $\partial f_{CO_2}/\partial P$ and $\partial f_{CO_2}/\partial T$ along the liquid + vapour curve of pure CO_2. Further experimental work along the L_{aq}–L_{CO_2}–V curve is desirable.

6.3. CO_2 solubility in the clathrate stability field

Fig. 5 shows isopleths of CO_2 solubility in water calculated by the corrected model (Eq. (10)), plotted with respect to other phase equilibria in the system. Regardless of the accuracy of the calculated isopleths, their equilibrium significance within the clathrate stability field needs careful consideration. As readily demonstrated by the Gibbs phase rule, the univariant bounding curve of clathrate stability (including Q_2) defines the only P–T conditions under which CO_2-rich fluids (vapour or liquid) can coexist at stable equilibrium with water and with clathrate. Consequently, at P–T conditions within the divariant stability field of clathrate, the solubility of aqueous CO_2 is no longer controlled by f_{CO_2} in the CO_2-vapour or CO_2-liquid. However, the dashed solubility curves shown in Figs. 5–7 are constructed on the assumption that this fugacity control does in fact obtain (Eq. (1)). The dashed curves consequently represent *metastable* equilibria that define aqueous CO_2 solubility under conditions of clathrate supersaturation (i.e. in the metastable absence of clathrate). Only one of the accepted experimental data (measured at 12 °C and 30.4 MPa by Wiebe and Gaddy [35]) corresponds to such metastable equilibrium. Wiebe and Gaddy [35] imply that they were able to sample the aqueous phase at this point just within the clathrate stability field (Fig. 3a), before clathrate formed in their experimental vessel.

The *stable* equilibrium values of aqueous CO_2 solubility in the clathrate field are not obviously defined by the experimental data considered so far, and they are not defined by our models. The plotted solubility curves are expected to be refracted at the clathrate bounding curve, as $f^0_{CO_2}$ in this non-stoichiometric compound takes over the buffering role of CO_2 dissolved in the coexisting water. Four of the experimental determinations of aqueous CO_2 solubility by Teng et al. [27] are reported to have been made in the presence of CO_2-clathrate (two measurements at 4.85 °C and two at 9.85 °C; Fig. 2). Teng et al. [27] claim that their measurements reflect stable equilibrium between water and CO_2-liquid at conditions within the divariant clathrate stability field, in apparent contradiction to the Gibbs phase rule. Being well aware of this contradiction, and having conducted time-resolved experiments, Teng et al. [27] argue that high diffusivity of CO_2 through the clathrate layer in their experimental apparatus allowed equilibrium with water to be established, while diffusion of H_2O into the CO_2-liquid through the clathrate layer was hindered by the large effective diameter of the H_2O clusters. Unfortunately, their datum for 9.85 °C at 6.44 MPa, which lies outside the clathrate stability field, contradicts the 12 °C data of Wiebe and Gaddy
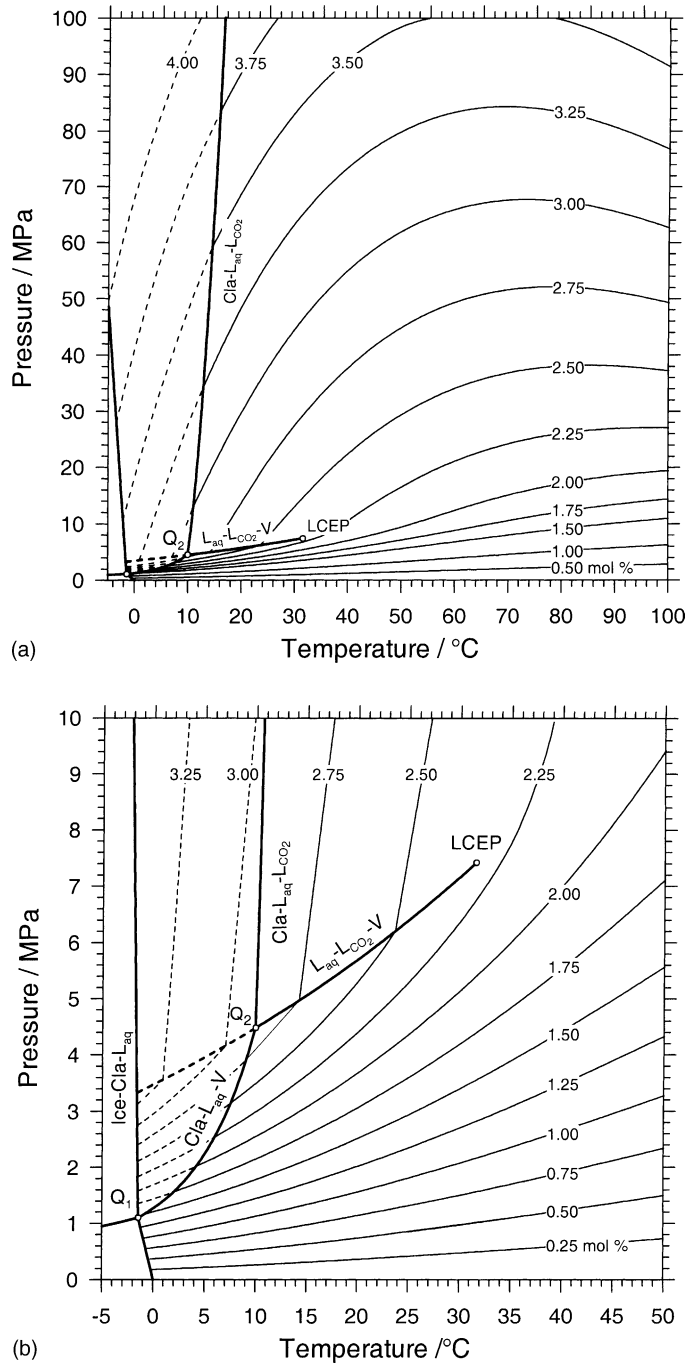
Fig. 5. *P–T* diagram showing selected solubility isopleths of $x_{CO_2(aq)}$ between 0.25 and 4 mol%, calculated by the corrected model (Eq. (10)). Water is stable over the entire contoured area. Metastable isopleths and phase boundaries within the clathrate stability field are shown dashed. See Fig. 1 for definition of phase-boundary labels. (a) Entire *P–T* region of model validity; (b) details of low-*P*, low-*T* region.

[35,36]; and hence, deviates from our fit significantly. The equilibrium significance of the remaining three measurements of Teng et al. within the clathrate field therefore remains equivocal from our point of view.

Several experimental studies have been made with the explicit aim of measuring aqueous CO_2 solubility in divariant equilibrium with CO_2-clathrate under *P–T* conditions deep within the clathrate stability field [25,31,48,49,51], as opposed to univariant conditions on the clathrate stability boundary. With the exception of the apparently erroneous results of [51] (see discussion in [52]), all these experiments show that isobaric CO_2 solubility dramatically *decreases* with decreasing temperature, in marked contrast to the dashed curves in Fig. 5. These results confirm that the dashed curves in Figs. 5–7 should indeed be interpreted as metastable equilibria.

The metastable extensions of the solubility isopleths (dashed curves in Figs. 4–6) are of little practical use in applications of our model calculations to systems at full equilibrium. However, the CO_2–H_2O system often exhibits considerable metastability in chemical and geochemical processes, and here the description of the metastable equilibria become useful. For example, Wendland et al. [10] traced the L_{aq}–L_{CO_2}–V curve down to $8\,^\circ C$ in a macroscopic system, whereas at complete equilibrium this phase assemblage is stable only above $9.93\,^\circ C$ (Q_2 in Fig. 1). In microscopic systems, such as fluid inclusions in minerals, the metastable L_{aq}–L_{CO_2}–V curve can be routinely observed down to $-20\,^\circ C$ [53]. Another case of practical application is when electrolytes are present in addition to CO_2 and H_2O. Here the stability
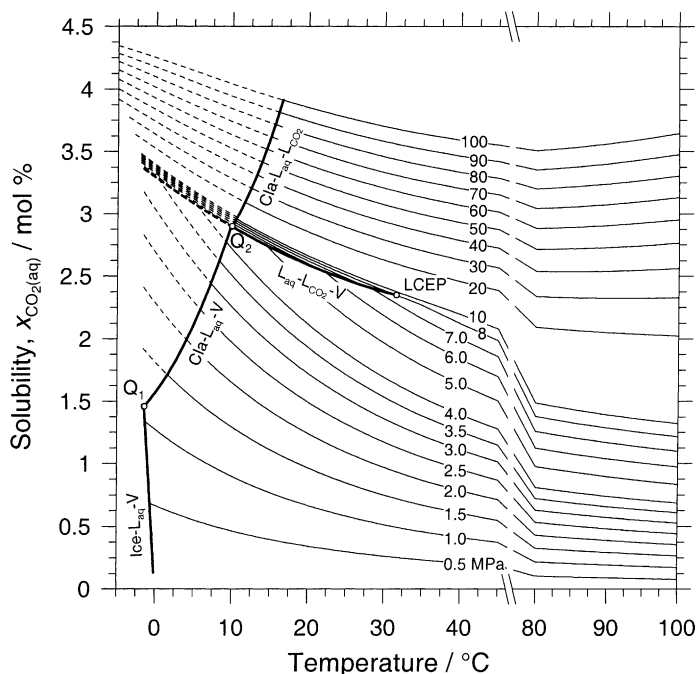

Fig. 6. T–$x_{CO_2(aq)}$ diagram showing selected solubility isobars between 0.5 and 100 MPa, calculated by the corrected model (Eq. (10)). Water is stable over the entire contoured area. Metastable isobars and phase boundaries within the clathrate stability field are shown dashed. See Fig. 1 for definition of phase-boundary labels. Note the break in scale of the *T*-axis between 44 and $80\,^\circ C$ (curves in this temperature interval are schematic, not quantitative).
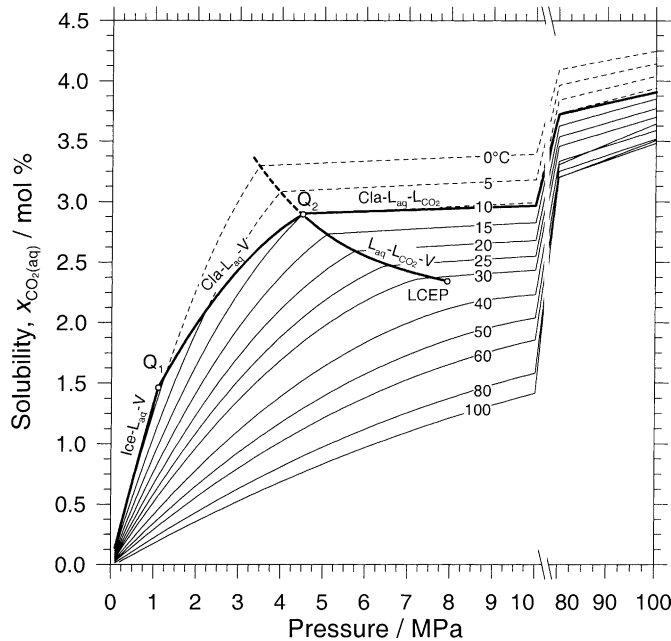
Fig. 7. P–$x_{CO_2(aq)}$ diagram showing selected solubility isotherms between 0 and 100 °C, calculated by the corrected model (Eq. (10)). Water is stable over the entire contoured area. Metastable isotherms and phase boundaries within the clathrate stability field are shown dashed. See Fig. 1 for definition of phase-boundary labels. Note the break in scale of the P-axis between 10 and 80 MPa (curves in this pressure interval are schematic, not quantitative). The intersection of the high-temperature isotherms near 85 MPa is due to the change in slope of the solubility isopleths at high pressures, as visible in Fig. 5a.

field of clathrate shrinks to lower temperatures as a function of electrolyte concentration. The dashed curves in Figs. 5–7 then serve as reference equilibria for the CO_2–H_2O binary at temperatures down to the specific clathrate stability limit, from which CO_2 solubilities in the CO_2–H_2O-electrolyte system may be calculated by means of salting-out parameters (e.g. [26]).

7. Conclusions

Our thermodynamic models of CO_2 solubility in pure water differ from previous approaches in that (1) a highly accurate EoS [13] is used to calculate f_{CO_2} in the CO_2-liquid and CO_2-vapour phases, (2) an improved EoS [45] is used to calculate Henry's law constants as a function of pressure and temperature, and (3) an empirical correction is applied to the basic Henry's law predictions for high pressures (high solubilities). The corrected model (Eq. (10)) is statistically a better description of the accepted experimental data than the basic Henry's law model. The derived correction function yields an expression for the temperature- and molality-dependence of the activity coefficient of $CO_{2(aq)}$ (Appendix A).

The corrected model is available as a computer code on the web-site <www.geo.unibe.ch/diamond>. In addition to providing CO_2 solubilities, the code calculates the full set of thermodynamic properties of the pure CO_2 and H_2O end-members, and of the CO_2-bearing aqueous solution between infinite dilution and CO_2-saturation, including activity coefficients, partial molar volume, absolute partial molar

entropy, partial molar heat capacity, chemical potential, Henry's law constant, bulk volume and bulk density.

We have not evaluated the performance of the models at conditions outside the upper P–T limits of the evaluated experimental database. At low temperatures the models should be applied only in the P–T region where aqueous solution is stable in the *absence* of clathrate, as delimited by the Ice–L_{aq}–V, Cla–L_{aq}–V and Cla–L_{aq}–L_{CO_2} curves in Fig. 5. Convenient polynomial functions describing CO_2 solubilities along the stability curves of clathrate and ice and along the L_{aq}–L_{CO_2}–V element are given by Eqs. (B.1)–(B.4) (Appendix B). At the low-pressure limit, the corrected model yields results that match those obtained using the model of Carroll et al. [3].

Our evaluation of reliability of the 25 available experimental studies resulted in rejection of 158 of the 520 data considered. Despite this 30% rejection rate, conflicts remain in the accepted set, and further experiments, especially along or near the L_{aq}–L_{CO_2}–V curve and in the region of CO_2-liquid stability are required to resolve these. No data remain to constrain the models within the stability field of CO_2–clathrate and only a few data are present at $P > 50$ MPa. In general, the predicted solubilities using the corrected model represent the accepted experimental data to within 2% (1 standard deviation). This precision is close to the inherent scatter in the accepted experimental data, of approximately 1.7% (1 standard deviation).

List of symbols

a	empirical parameter of the equation of state for dissolved CO_2 ($cm^3\,g^{-1}$)
a_{ij}	polynomial coefficients (Eq. (8))
b	empirical parameter of the equation of state for dissolved CO_2 ($cm^3\,K^{0.5}\,g^{-1}$)
Cla	solid CO_2-clathrate-hydrate
$f^0_{CO_2(P,T)}$	fugacity of pure CO_2 at specified P–T conditions (MPa)
$f^0_{H_2O}$	fugacity of pure H_2O (MPa)
$k_{H(P,T)}$	Henry constant of CO_2 in pure water at specified P–T conditions (MPa)
L	liquid phase
LCEP	lower critical end-point
P	pressure (MPa)
P_{CO_2}	partial pressure of CO_2 (MPa)
P_{total}	total pressure (MPa)
$P_{watersat}$	pressure of liquid-water equilibrium of pure H_2O (MPa)
Q	quadruple point
r^*	empirical correction function (Eq. (9))
r_0	relative error in CO_2 solubility associated with our basic model (Eq. (6))
R	gas constant (8.31441 $cm^3\,MPa\,K^{-1}\,mol^{-1}$)
t	temperature ($°C$)
T	temperature: in equations in K, in text in $°C$
V	CO_2-rich vapour phase
w_i	weight assigned to datum i
$x_{CO_2(aq)}$	concentration of dissolved CO_2 in aqueous phase (mol%)
$x_{corr.}$	corrected CO_2 solubility (Eq. (10)) (mol%)
$x_{exper.}$	experimental CO_2 solubility for a specific datum (mol%)
x_{model}	CO_2 solubility (mol%) predicted according to Eq. (2)
y	concentration of dissolved CO_2 in CO_2-rich phase (mol%)

Greek letters

$\gamma_{CO_2(aq)}$ unsymmetric activity coefficient of dissolved CO_2 in aqueous phase (Henry's law behaviour)

γ_y activity coefficient of CO_2 in CO_2-rich phase

$\rho_{H_2O}^0$ density of pure H_2O ($g\,cm^{-3}$)

σ weighted standard deviation of the relative solubility errors

ξ empirical parameter of the equation of state for dissolved CO_2

Subscripts

aq   aqueous solution

liq   liquid phase

vap   vapour phase

Acknowledgements

Appendix A

It is useful to convert the activity coefficient of aqueous CO_2 from the mole-fraction scale, as used in Eq. (2) and in the above derivations, to the molal scale. Eq. (12) gives the Henry's law activity coefficient of aqueous CO_2 on a mole-fraction scale, γ_H:

$$\gamma_H = \frac{x_{model}}{x_{corr.}} = (1 + r^*)^{-1}. \tag{12}$$

This form of the activity coefficient can be converted to the Henry's law molal scale by equating the corresponding expressions for the chemical potential of dissolved CO_2 on the two scales:

$$\mu_g^0(T) + RT\ln(\gamma_H) + RT\ln(x) + RT\ln(k_H) = \mu_m^0(T, P) + RT\ln(m) + RT\ln(\gamma_m) \tag{A.1}$$

and using the definition of the Henry constant, k_H (in MPa), at given pressure P (in MPa) and temperature T (in K)

$$\ln k_H = \ln 55.508 + \frac{\mu_{m(P,T)}^0 - \mu_{g(T)}^0}{RT}, \tag{A.2}$$

we obtain

$$\ln(\gamma_H) + \ln(x) + \ln 55.508 = \ln(m) + \ln(\gamma_m). \tag{A.3}$$

Here $\mu_{g(T)}^0$ and $\mu_{m(P,T)}^0$ are the standard chemical potentials of CO_2 in the gaseous phase (pure perfect gas at 0.1 MPa) and in the aqueous solution (infinite dilution at $1\,mol\,kg^{-1}$ of H_2O solvent), respectively, and x and m are the mole fraction and the molality of aqueous CO_2.

Since

$$m_2 = 55.508 \frac{x_2}{1 - x_2}, \tag{A.4}$$

we finally arrive at

$$\ln \gamma_m = \ln \gamma_H + \ln(1 - x) = -\ln(1 + r^*) + \ln(1 - x_2). \tag{A.5}$$

For convenience of application, the polynomial Eq. (9) for r^* is rearranged into the following equivalent form to express the dependence of $\ln \gamma_m$ on temperature (T in K) and on the molality of aqueous CO_2 at CO_2-saturation (m):

$$\ln \gamma_m = (-0.099085 + 0.48977 \times 10^{-3}T - 0.962628 \times 10^{-6}T^2)m$$
$$+ (0.218384 - 1.024319 \times 10^{-3}T + 1.222992 \times 10^{-6}T^2)m^2 \tag{A.6}$$

with the limits of validity being $271\,\text{K} \leq T \leq 373\,\text{K}$ and $0 \leq m \leq 2.5$.

Appendix B

To facilitate application of the corrected model, the following polynomial expressions describe aqueous CO_2 solubility as a function of temperature along four of the univariant phase boundaries shown in Fig. 5b:

(1) Solubility along the coexistence curve of aqueous liquid+CO_2-rich liquid+CO_2-rich vapour (labelled L_{aq}–L_{CO_2}–V in Fig. 1), including the *metastable* extension below Q_2 at 9.93 °C:

$$x_{CO_2(aq)} = 3.292396 - 4.631694 \times 10^{-2}t + 6.782674 \times 10^{-4}t^2$$
$$- 7.297968 \times 10^{-6}t^3 + 7.003483 \times 10^{-8}t^4, \tag{B.1}$$

where $x_{CO_2(aq)}$ is the solubility of aqueous CO_2 in mol%, and t is temperature between 0 °C and the LCEP at 31.48 °C. This equation represents metastable, clathrate-supersaturated equilibrium between 0 and 9.93 °C. Note that the P–T locus of the L_{aq}–L_{CO_2}–V curve for the CO_2–H_2O binary is slightly different from that of the L_{CO_2}–V curve for pure CO_2 [10,13]. However, the P–T differences are insignificant in the present context, as they correspond to differences in aqueous CO_2 solubility that are smaller than the precision of our model.

(2) Solubility along the coexistence curve of CO_2-clathrate-hydrate + aqueous liquid + CO_2-rich vapour (labelled Cla–L_{aq}–V in Figs. 1 and 5–7):

$$x_{CO_2(aq)} = 1.570415 + 7.887505 \times 10^{-2}t + 4.734722 \times 10^{-3}t^2 + 4.56477 \times 10^{-4}t^3$$
$$- 3.796084 \times 10^{-5}t^4, \tag{B.2}$$

where $x_{CO_2(aq)}$ is the solubility of aqueous CO_2 in mol%, and t is temperature in °C along the clathrate stability boundary between −1.48 °C (Q_1 point) and 9.93 °C (Q_2 point).

(3) Solubility along the coexistence curve of CO_2-clathrate-hydrate + aqueous liquid + CO_2-rich liquid (labelled Cla–L_{aq}–L_{CO_2} in Figs. 1 and 5–7):

$$x_{CO_2(aq)} = 8.912032 - 1.955046t + 2.215544 \times 10^{-1}t^2 - 1.053749 \times 10^{-2}t^3$$
$$+ 1.9241 \times 10^{-4}t^4, \tag{B.3}$$

where $x_{CO_2(aq)}$ is the solubility of aqueous CO_2 in mol%, and t is temperature in °C along the clathrate stability boundary between the 9.93 °C (Q_2 point) and 16.6 °C (at 100 MPa).

(4) Solubility along the coexistence curve of ice + aqueous liquid + vapour (labelled Ice–L_{aq}–V in Figs. 1 and 5–7):

$$x_{CO_2(aq)} = 4.557142 \times 10^{-3} - 1.043041t - 3.906477 \times 10^{-2}t^2, \tag{B.4}$$

where $x_{CO_2(aq)}$ is the solubility of aqueous CO_2 in mol%, and t is temperature between -0.125 °C (at 0.1 MPa) and -1.48 °C (Q_1 point).

References

[1] L.W. Diamond, Lithos 55 (2000) 69–99.
[2] Y. Krüger, L.W. Diamond, Chem. Geol. 173 (2001) 159–177.
[3] J.J. Carroll, J.D. Slupsky, A.E. Mather, J. Phys. Chem. Ref. Data 20 (1991) 1201–1209.
[4] R. Crovetto, J. Phys. Chem. Ref. Data 20 (1991) 575–589.
[5] W.S. Dodds, L.F. Stutzman, B. Sollami, Ind. Eng. Chem. Chem. Eng. Data Ser. 1 (1956) 92–95.
[6] P. Scharlin, in: J.W. Lorimer (Ed.), IUPAC Solubility Data Series, vol. 62, Oxford University Press, Oxford, 1996, 383 pp.
[7] S.D. Larson, Phase studies of the two-component carbon dioxide–water system involving the carbon dioxide hydrate, Ph.D. Thesis, University of Illinois, 1955, 84 pp.
[8] S. Takenouchi, G.C. Kennedy, J. Geol. 73 (1965) 1–55, 383–390.
[9] H.-J. Ng, D.B. Robinson, Fluid Phase Equilib. 21 (1985) 145–155.
[10] M. Wendland, H. Hasse, G. Maurer, J. Chem. Eng. Data 44 (1999) 901–906.
[11] K.Y. Song, R. Kobayashi, SPE Form. Eval. 2 (1987) 500–508.
[12] G. Morrison, J. Phys. Chem. 85 (1981) 759–761.
[13] R. Span, W. Wagner, J. Phys. Chem. Ref. Data 25 (1996) 1509–1596.
[14] K. Tödheide, E.U. Franck, Z. Phys. Chemie Neue Folge 37 (1963) 387–401.
[15] S. Takenouchi, G.C. Kennedy, Am. J. Sci. 262 (1964) 1055–1074.
[16] S.M. Sterner, R.J. Bodnar, Am. J. Sci. 291 (1991) 1–54.
[17] S.V. Wroblewski, Ann. Phys. Chem. 18 (1883) 290–308.
[18] G.K. Anderson, J. Chem. Eng. Data 47 (2002) 219–222.
[19] W. Sander, Z. Phys. Chem., Stoechiom. Verwandtschaftsl. 78 (1912) 513–549.
[20] R. Vilcu, I. Gainar, Revue Romaine de Chimie 12 (1967) 181–189.
[21] I.R. Kritschewsky, N.M. Shaworonkoff, V.A. Aepelbaum, Z. Phys. Chem. A 175 (1935) 232–238.
[22] P.C. Gillespie, G.M. Wilson, Vapor–liquid and liquid–liquid equilibria: water–methane, water–carbon dioxide, water–hydrogen sulfide, water–*n*-pentane, water–methane–*n*-pentane, Gas Processors Association, Tulsa, Research Report RR48, 1982.
[23] O. Hähnel, Centr. Min. Geol. 25 (1920) 25–32.
[24] P.B. Stewart, P. Munjal, J. Chem. Eng. Data 15 (1970) 67–71.
[25] P. Servio, P. Englezos, Fluid Phase Equilib. 190 (2001) 127–134.
[26] S.D. Cramer, The solubility of methane, carbon dioxide, and oxygen in brines from 0 to 300 °C, US Bureau of Mines Report of Investigations, vol. 8706, 1982.
[27] H. Teng, A. Yamasaki, M.-K. Chun, H. Lee, J. Chem. Thermodyn. 29 (1997) 1301–1310.
[28] R.A. Shagiakhmetov, A.A. Tarzimanov, Deposited Document SPSTL 200 khp—D 81—1982 (1981).
[29] P.M. Oleinik, Neftepromyslovoe Delo, vol. 8, p. 7 (in Russian), cited in [30].
[30] A.Y. Namiot, Solubility of Gases in Water, Nedra, Moscow, 1991 (in Russian).
[31] S.O. Yang, I.M. Yang, Y.S. Kim, C.S. Lee, Fluid Phase Equilib. 175 (2000) 75–89.
[32] Y.D. Zel'vinskii, Zhurn. Khim. Prom. 14 (1937) 1250–1257 (in Russian).
[33] S.D. Malinin, N.I. Savelyeva, Geochem. Int. 9 (1972) 410–418.
[34] S.D. Malinin, N.A. Kurovskaya, Geochem. Int. 12 (1975) 199–201.

[35] R. Wiebe, V.L. Gaddy, J. Am. Chem. Soc. 62 (1940) 815–817.
[36] R. Wiebe, V.L. Gaddy, J. Am. Chem. Soc. 61 (1939) 315–318.
[37] E. Bartholomé, H. Friz, Chem. Ing. Tech. 28 (1956) 706–708.
[38] J. Matous, J. Sobr, J.P. Novak, J. Pick, Collect. Czech. Chem. Commun. 34 (1969) 3982–3985.
[39] A. Zawisza, B. Malesinska, J. Chem. Eng. Data 26 (1981) 388–391.
[40] G. Müller, E. Bender, G. Maurer, Ber. Bunsenges. Phys. Chem. 92 (1988) 148–160.
[41] M.B. King, A. Mubarak, J.D. Kim, T.R. Bott, J. Supercritical Fluids 5 (1992) 296–302.
[42] A. Bamberger, G. Sieder, G. Maurer, J. Supercritical Fluids 17 (2000) 97–110.
[43] R. Kruse, E.U. Franck, Ber. Bunsenges. Phys. Chem. 86 (1982) 1036–1038.
[44] R. Wiebe, V.L. Gaddy, J. Am. Chem. Soc. 63 (1941) 475–477.
[45] N.N. Akinfiev, L.W. Diamond, Geochim. Cosmochim. Acta 67 (2003) 613–629.
[46] P.G. Hill, J. Phys. Chem. Ref. Data 19 (1990) 1233–1274.
[47] J.A. Barbero, L.G. Hepler, K.G. McCurdy, P.R. Tremaine, Can. J. Chem. 61 (1983) 2509–2519.
[48] I. Aya, K. Yamane, H. Nariai, Energy 22 (1997) 263–271.
[49] O.Y. Zatsepina, B.A. Buffett, Fluid Phase Equilib. 192 (2001) 85–102.
[50] R. Wiebe, V.L. Gaddy, C. Heins, J. Am. Chem. Soc. 55 (1933) 947–953.
[51] H. Teng, A. Yamasaki, J. Chem. Eng. Data 43 (1998) 2–5.
[52] R. Ohmura, Y.H. Mori, J. Chem. Eng. Data 44 (1999) 1432–1433.
[53] L.W. Diamond, Geochim. Cosmochim. Acta 55 (1992) 273–280.